Available online at www.sciencedirect.com
SCIENCE DIRECT®
ELSEVIER
Applied Surface Science 208–209 (2003) 61–70
applied surface science
www.elsevier.com/locate/apsusc

Theoretical approach to the laser-induced melting of graphite under different pressure conditions

Martin E. Garcia[a,*], Harald O. Jeschke[b]

[a]*Institut für Theoretische Physik der Freien, Universität Berlin, Arnimallee 14, Berlin 14195, Germany*
[b]*Department of Physics and Astronomy, Rutgers University, 136 Frelinghuysen Road, Piscataway, NJ 08854-8019, USA*

Abstract

We present a theoretical study of the laser-induced femtosecond melting of (1) graphite under high external pressure and (2) ultrathin graphite films under normal conditions. Our approach consists of molecular dynamic simulations performed on the basis of a time-dependent, many-body potential energy surface derived from a tight-binding Hamiltonian. Our results show that the laser-induced melting process occurs in two steps: (i) destruction of the graphite sheets via bond breaking, and (ii) merging of the melted layers. The separation of the two steps is more evident for graphite under pressure (10 GPa), but is also present in graphite films at normal pressure. The melting product is a low-density carbon phase, which remains stable under high pressure, but is unstable with an ultrashort life-time under normal pressure.

Keywords: Laser-induced melting; Graphite; Molecular dynamic simulation

1. Introduction

The irradiation of solids with femtosecond lasers leads to interesting ultrafast phenomena as, for example, ultrafast phase transitions [1–10], ablation [11–14], excitation of coherent phonons [15], and optical breakdown [16].

It is now well established, that subpicosecond laser pulses induce in the irradiated materials effects which qualitatively differ from those produced by long pulses with durations of several tens of pico- or nanoseconds. In particular, the processes leading to a melting of graphite are of high fundamental interest. The thermal melting has already been studied intensively. In contrast, theoretical studies of laser-induced non-equilibrium melting of graphite have only started recently [7,17,18]. In a previous paper, we have shown that intense femtosecond pulses induce bond-breaking processes inside the graphite layers and lead to ultrafast melting and expansion of the system, the intermediate liquid state induced by the laser showing signatures corresponding to low-density liquid carbon (LDLC) [7]. In this paper, we carefully analyze the mechanisms of the non-equilibrium melting of graphite upon femtosecond laser excitation. As initial state we consider graphite under different external pressure conditions. We show that, in the case of thin films under normal pressure conditions, the liquid phase induced by the laser has a very short life time and constitutes an intermediate state which is followed by vaporization and ablation. When graphite is subject to high external pressure (10 GPa), the laser excitation merely induces the melting process. We study the different stages of the melting process.

* Corresponding author.
E-mail addresses: garcia@physik.fu-berlin.de (M.E. Garcia), jeschke@physics.rutgers.edu (H.O. Jeschke).

0169-4332/02/$ – see front matter
doi:10.1016/S0169-4332(02)01337-5

This study is important for a great number of experiments where non-equilibrium conditions are induced in carbon materials.

The paper is organized as follows. In Section 2, we sketch our theoretical approach. In Section 3, we present and discuss the results of our simulations. Finally, in Section 4 we briefly summarize our work.

2. Theory

We employ a molecular dynamics method on the basis of an electronic tight-binding Hamiltonian. This real-space calculation takes into account all atomic degrees of freedom within a unit cell of typically 100–1000 atoms. Special attention is paid to the strong non-equilibrium conditions created in the electronic system by the ultrashort laser pulse. A method of calculating non-equilibrium occupation numbers for the energy levels of the system leads to a molecular dynamics calculation on time-dependent potential energy surfaces. This approach provides a theoretical framework for the treatment of laser-induced non-equilibrium situations in materials where atomic and electronic degrees of freedom play an equally important role.

The key quantity in our approach is the potential energy surface $U(\boldsymbol{r}_{ij}, t)$ for the motion of the atoms, which is a many-body potential depending in a complex form on the interatomic distances $\boldsymbol{r}_{ij}$ and on time (due to the presence of the external field). Since the laser primarily excites electrons, the function $U(\boldsymbol{r}_{ij}, t)$ must be derived from an electronic model.

Therefore, we start from the Hamiltonian

$$H = H_{\mathrm{TB}} + \sum_{i<j} \phi(r_{ij}), \tag{1}$$

where the second term contains a repulsive potential $\phi(r_{ij})$ that takes care of the repulsion between the ionic cores, and the first term is a tight-binding Hamiltonian

$$H_{\mathrm{TB}} = \sum_{i\eta} \epsilon_{i\eta} n_{i\eta} + \sum_{\substack{ij\eta\vartheta \\ j\neq i}} t_{ij}^{\eta\vartheta}(\boldsymbol{r}_{ij}) c_{i\eta}^{+} c_{j\vartheta}. \tag{2}$$

Here, the first term is the on-site contribution. $\epsilon_{i\eta}$ refers to the electronic level on atom i, orbital η. We consider one s- and three p-orbitals per site. $n_{i\eta}$ is the corresponding electron occupation. In the second term, the $t_{ij}^{\eta\vartheta}$ are the hopping integrals, which depend on the interatomic distances, and $c_{i\eta}^{+}$ and $c_{j\vartheta}$ are creation and annihilation operators for an electron at site i or j in orbitals η or ϑ, respectively.

From the Hamiltonian of Eq. (1), we calculate forces using the Hellman–Feynman theorem:

$$\boldsymbol{f}_k(\{r_{ij}(t)\}, t) = -\nabla_k \left[\sum_m n(\epsilon_m, t) \langle m | H_{\mathrm{TB}}(\{r_{ij}(t)\}) | m \rangle + \sum_{i<j} \phi(r_{ij}) - T_{\mathrm{e}}(t) S_{\mathrm{e}}(t) \right]. \tag{3}$$

Here, $|m\rangle$ stands for the eigenvector of the Hamiltonian H_{TB} that corresponds to the eigenvalue ϵ_m. The third term contains the electronic temperature $T_{\mathrm{e}}(t)$ and the electronic entropy $S_{\mathrm{e}}(t)$. The special feature of the theory which makes it applicable to optically excited materials is contained in the time-dependent occupation numbers $n(\epsilon_m, t)$ for the energy levels ϵ_m of the system. While in thermal equilibrium these occupation numbers are calculated from a Fermi–Dirac distribution function $n^0(\epsilon_m) = 2/(1 + \exp\{(\epsilon_m - \mu)/k_{\mathrm{B}} T_{\mathrm{e}}\})$ at a given electronic temperature T_{e}, electronic non-equilibrium is accounted for by solving equations of motion for the occupation of electronic states:

$$\frac{\mathrm{d}n(\epsilon_m, t)}{\mathrm{d}t} = \int_{-\infty}^{\infty} \mathrm{d}\omega\, g(\omega, t - \Delta t) \{ [n(\epsilon_m - \hbar\omega, t - \Delta t) + n(\epsilon_m + \hbar\omega, t - \Delta t) - 2n(\epsilon_m, t - \Delta t)] \} - \frac{n(\epsilon_m, t) - n^0(\epsilon_m)}{\tau_1}. \tag{4}$$

Thus, the electronic distribution is at each time step folded with the pulse intensity function $g(\omega, t)$. This means that, at each time step, the occupation of an energy level ϵ_m changes in proportion to the occupation difference with respect to levels at $\epsilon_m - \hbar\omega$ and at $\epsilon_m + \hbar\omega$. In Eq. (4), constant optical matrix elements are assumed. The second term of Eq. (4) describes the electron–electron collisions that lead to an equilibration of the electronic system with a rate equation of the Boltzmann type for the distribution $n(\epsilon_m, t)$. Hence, with a time constant τ_1, the distribution $n(\epsilon_m, t)$ approaches a Fermi–Dirac distribution $n^0(\epsilon_m)$.

The electron temperature T_{e} that results from the electron thermalization will not remain constant over time but will decrease due to electron–phonon coupling

and to diffusion of hot electrons out of the laser-excited region of the solid into colder areas. In the regime of an excitation of typically 10% of the valence electrons into the conduction band for which this theory is intended, no precise knowledge about thermal conductivity of the electrons and electron–phonon coupling constants is available. Thus, a relaxation time τ_2 which characterizes the time scale of the total decrease of the electron temperature by both the electron–phonon interaction and by the hot electron diffusion processes is assumed:

$$\frac{dT_e(t)}{dt} = -\frac{T_e(t) - T(t)}{\tau_2}. \quad (5)$$

This simple relaxation time approach has the advantage that the time scale τ_2 on which the electron–lattice equilibration takes place can be taken from experiment. We use a value of $\tau_2 = 4.4$ ps

The forces can now be used to solve the equations of motion for the atoms numerically. In the case of a bulk system, a constant pressure molecular dynamics (MD) scheme is used. Constant pressure means that the external pressure acting on the sample remains constant. Of course, the internal pressure of the system will not remain unchanged. Moreover, it will dramatically increase as a consequence of the laser excitation. These changes in the internal pressure are taken into account in our approach. The molecular dynamics

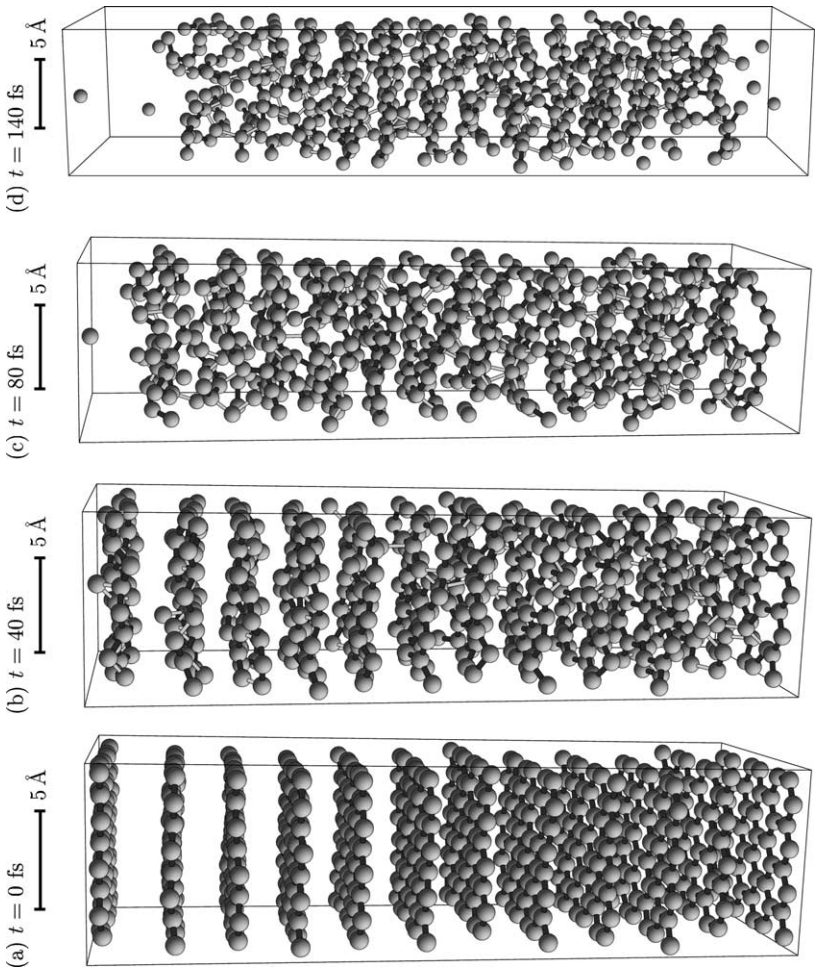

Fig. 1. Short-time structural response of a graphite film at an absorbed energy of $E_0 = 4.0$ eV per atom. The laser-pulse duration was $\tau = 20$ fs. This figure shows the early stages of the formation of a transient, low-density liquid carbon phase.

at constant external pressure are based on a Lagrangian which contains the shape and size of the molecular dynamics supercell as additional degrees of freedom [19]:

$$L = \sum_{i=1}^{N} \frac{m_i}{2} \dot{\boldsymbol{s}}_i^{\mathrm{T}} h^{\mathrm{T}} h \dot{\boldsymbol{s}}_i + K_{\mathrm{cell}} - \Phi(\{r_{ij}\}, t) - U_{\mathrm{cell}}. \quad (6)$$

The first term is the kinetic energy of the atoms, with the coordinates of the atoms $\boldsymbol{r}_i = h\boldsymbol{s}_i$ written in terms of the relative coordinates $\boldsymbol{s}_i$ and the 3×3-matrix h that contains the vectors spanning the MD supercell; $\dot{\boldsymbol{s}}_i$ are the relative velocity vectors, and T denotes transposition. $\Phi(\{r_{ij}\}, t)$ is the potential which is calculated from a tight-binding formalism as explained above.

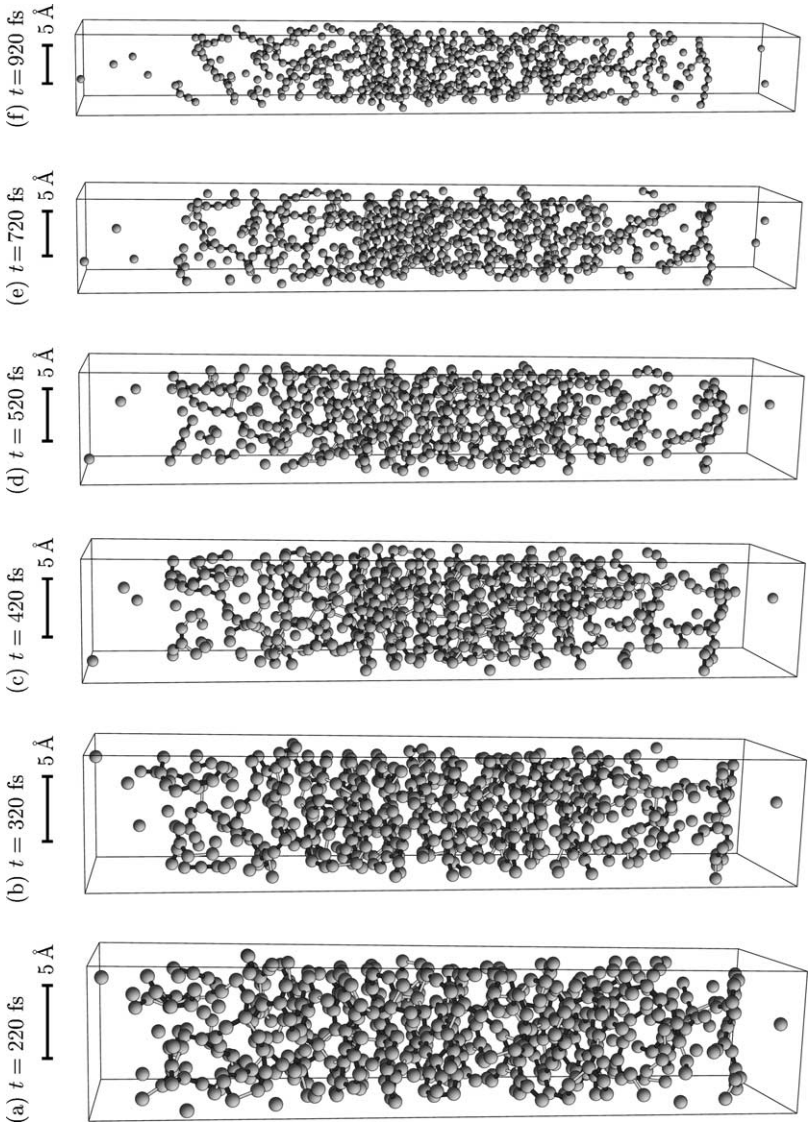

Fig. 2. Ablation of a graphite film at an absorbed energy of $E_0 = 4.0$ eV per atom. The laser-pulse duration was $\tau = 20$ fs. This figure shows the advanced stages of the ablation process (for the early stages see Fig. 1). Four emitted carbon monomers far from the surface are not shown. A strong expansion of the material is observed; as the film has been represented with constant height, this is apparent from the narrowing of the columns. The material is in strong, liquid-like motion. In (d)–(f), in addition to the emission of carbon monomers, linear carbon chains are formed and emitted.

The terms in the Lagrangian of Eq. (6), which are responsible for the simulation of constant external pressure, are an additional kinetic energy term K_{cell} for which the simplest form is $K_{\text{cell}} = (w_{\text{cell}}/2)\text{Tr}(\dot{h}^{\text{T}}\dot{h})$ [19], and U_{cell} is an additional potential term which describes the effect of an isotropic external pressure $U_{\text{cell}} = p_{\text{ext}}\Omega$; $\Omega = \det(h)$ is the volume of the MD supercell. The equations of motion are derived from Eq. (6) by the Euler–Lagrange formalism, and they are integrated numerically with the velocity form of the Verlet algorithm [20].

3. Results

Based on the approach presented in the previous section we have performed different simulations to describe the structural response of ultrathin graphite

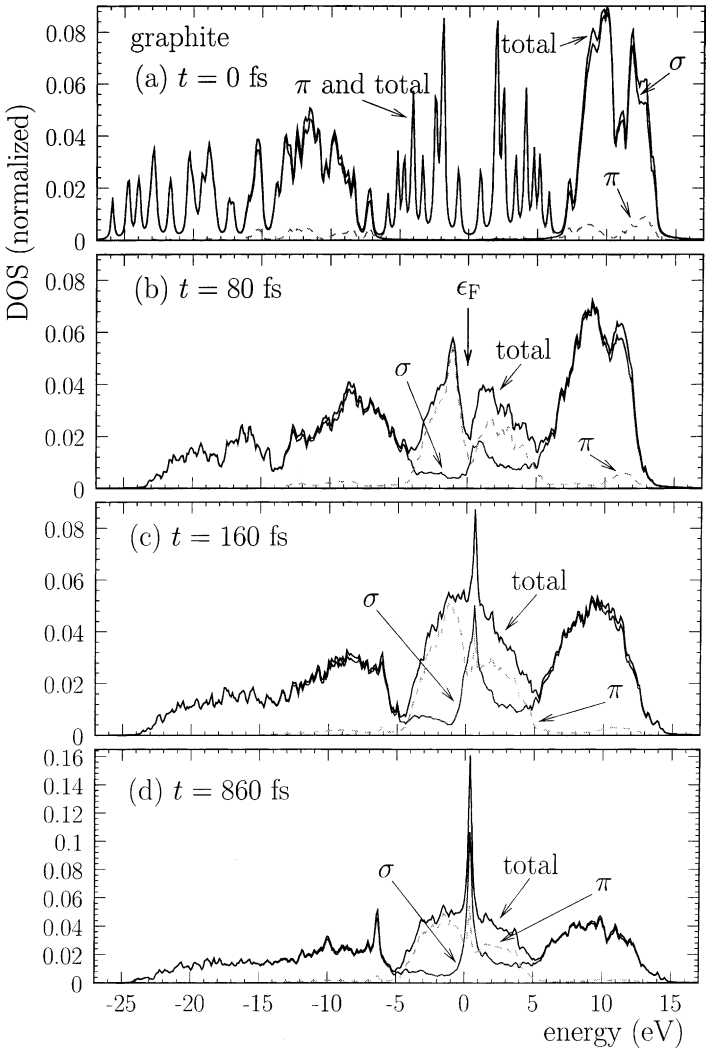

Fig. 3. Densities of states for the ablation of graphite at an absorbed energy of $E_0 = 4.0$ eV per atom. This figure corresponds to the trajectory of Figs. 1 and 2. The π contribution to the DOS is indicated by a dashed line. The features of the graphite DOS in (a) at $t = 0$ fs are quickly replaced by a metallic-like DOS (b). The sharp peak at the Fermi level that appears at $t = 160$ fs in (c) is due to contributions of linear carbon chains. Note, the ordinate scale of (d) is different from (a) to (c).

films and bulk graphite under pressure to femtosecond laser pulses.

In Figs. 1 and 2 we show snapshots of a long trajectory of a thin graphite film in which melting and subsequent evaporation and ablation can be observed. The film consists of $N = 576$ atoms. The snapshots shown are for a laser pulse with a Gaussian amplitude $A(t) = \exp\{-4 \ln 2\, t^2/\tau^2\}$ in time ($\tau = 20$ fs) and such an intensity that the energy absorbed by the system is $E_0 = 4.0$ eV per atom. This energy density is high enough to break the bonds of the graphite planes. After $t = 40$ fs, we see that especially in the lower part of the film, bonds are formed between the graphite planes. Note, the initial graphite film was thermalized to $T = 300$ K, so that at the time the laser pulse hits the material all atoms are in an individual state of motion. This determines the initial conditions for the amplified oscillations due to the presence of the electron-hole plasma. Thus, it is not surprising that on a very short time scale there are differences in the motion of different graphite planes. At $t = 80$ fs, we can see already the first carbon monomer being evaporated from the material, confirming that the graphite planes have been excited above their cohesion threshold. In the following snapshot at $t = 140$ fs, the graphite planes have been dissolved completely and a liquid has been formed.

In Fig. 2, the further time development of the excited graphite sample of Fig. 1 is shown. In the snapshots presented here, a strong volume expansion is observed, e.g. from 5480 Å^3 at $t = 220$ fs to 6040 Å^3 at $t = 320$ fs. This expansion is reflected in Fig. 2 in the decreasing width of the column of the material rather than in an increasing z extension of the column which would have made for an awkward representation in the figures. In all graphs of Fig. 2, four monomers that had already moved far away from the surface were omitted. Fig. 2 now shows the advancing ablation process. Between $t = 420$ and 920 fs we can observe how the expansion of the material takes place especially rapidly in the two surface regions of the film, leading to low densities

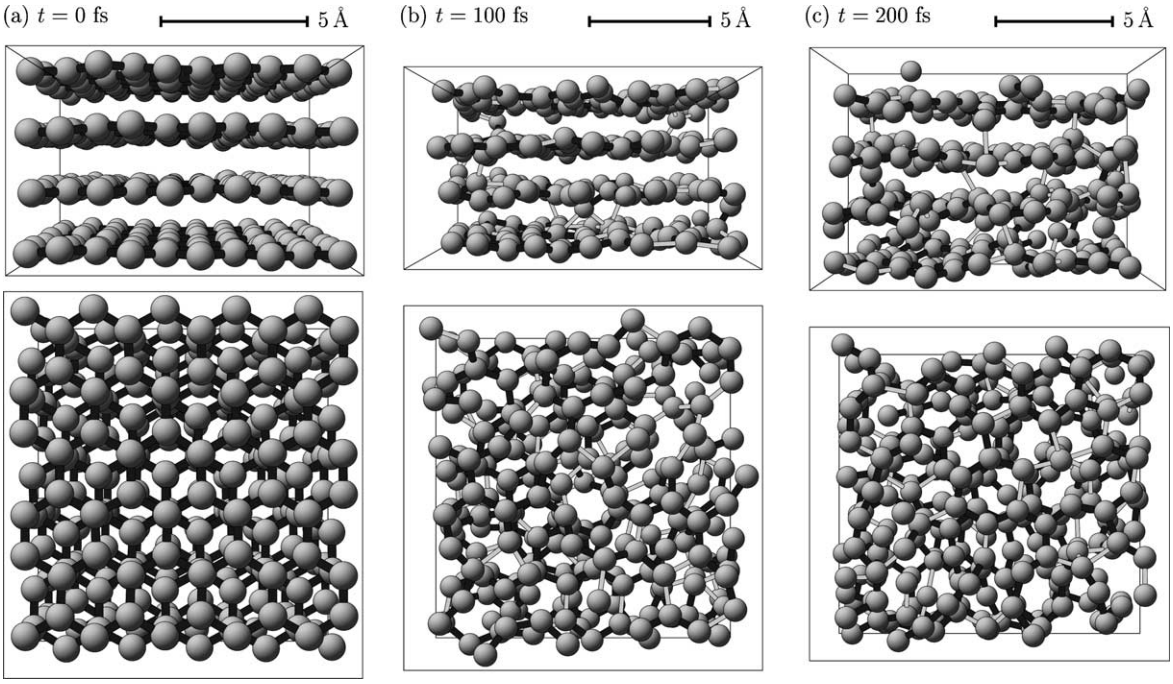

Fig. 4. Early stage of the melting of graphite under a pressure of $p = 10$ Gpa at an absorbed energy of $E_0 = 3.8$ eV per atom. The pulse duration was $\tau = 20$ fs. At each time the MD unit cell is shown from above and from the side. Bonds up to a length of $l = 1.6$ Å are drawn in dark grey, weaker bonds of 1.6 Å $< l <$ 2.0 Å in light grey. The early stage of melting is characterized by the loss of order in the graphite planes, while only little interaction between the planes takes place.

and the formation of short carbon chains which then start to leave the sample.

In Fig. 3 we show the densities of state that correspond to Figs. 1 and 2. At $t = 80$ fs (see Fig. 3b) the features of the graphite DOS have already significantly broadened, and at the Fermi level the DOS has increased. In Fig. 3c for $t = 160$ fs, the DOS has become metallic-like. The sharp spike close to the Fermi level corresponds to features of the DOS of the linear chain. These features have developed further in Fig. 3d for $t = 860$ fs.

We now analyze in detail the transient liquid phase induced, whose formation is shown in Fig. 1. Note, because of the expansion of the film this liquid phase has a low density and is characterized by the presence of carbon chains. To characterize this laser-induced liquid phase we have determined the order parameter $\Psi = (\rho_4 - \rho_2)/(\rho_4 + \rho_2)$ which was proposed by Glosli and Ree [21] to distinguish between the high- and the low-density liquid phase of carbon. Here, ρ_2 and ρ_4 correspond to the densities of two- and four-fold coordinated carbon atoms determined fol-

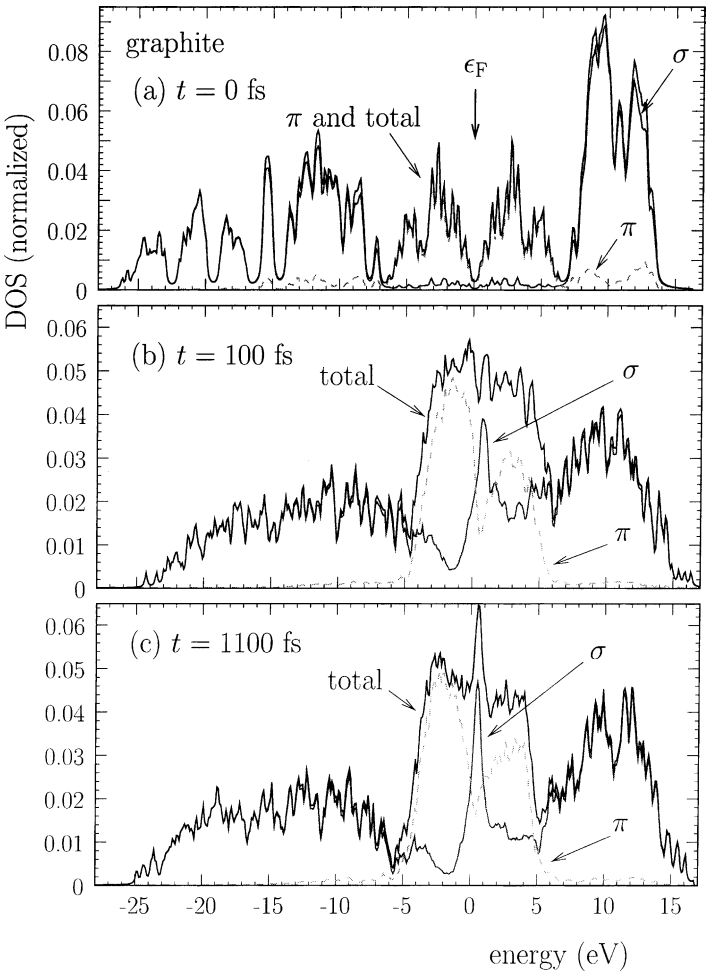

Fig. 5. Densities of states for the melting of graphite under a pressure of $p = 10$ GPa. This figure corresponds to the trajectory of Figs. 4 and 6. The π contribution to the DOS is indicated by a dashed line. The graphite DOS which is still present at $t = 0$ fs (the time of the maximum of the laser pulse of $\tau = 20$ fs duration) changes rapidly to a metallic-like DOS in (b). (c) It shows the DOS 1 ps later. Except for a sharp peak close to the Fermi level the overall shape of the DOS has not changed.

lowing Brenner [22]. By averaging the quantity Ψ in time up to $t = 1$ ps after the pulse maximum, we find a value of $\Psi = -0.8$. This confirms that a low-density, predominantly two-fold coordinated liquid carbon phase was produced by the laser excitation. This liquid carbon phase is unstable and has an ultrashort lifetime, as can be seen in Fig. 2. It is interesting to point out that this unstable liquid phase is formed during a transient state in which the energy redistribution has only partially taken place. Therefore, it is essentially caused by a non-thermal process and is not directly related to the formation of a superheated, metastable liquid reported by Sokolowski-Tinten et al. [12]. Such processes occur at much longer time scales and lower laser intensities.

In the following we discuss the laser-induced formation of liquid carbon for graphite under high pressure.

Fig. 4 shows the first stage of non-equilibrium melting of graphite under $p = 10$ GPa. It was calculated with an MD supercell of $N = 240$ atoms. The pressure was applied already in the simulated annealing process of the hexagonal graphite so that a fully equilibrated sample at $T = 300$ K and $p = 10$ GPa is used for this calculation. The laser pulse had $\tau = 20$ fs duration and an energy $E_0 = 3.8$ eV per atom was absorbed. Note, this absorbed energy is not far above the damage threshold of graphite. Indeed, in a trajectory of the same material which absorbed $E_0 = 3.3$ eV per atom no melting was observed during the first 2 ps. In Fig. 4 the MD supercell is shown from above and from the side. We observe that already at $t = 100$ fs (see Fig. 4b) the honey comb structure of the graphite planes has been destroyed. Nevertheless, up to a time $t = 200$ fs (see Fig. 4c) the graphite planes show almost no interaction, and the layered structure of the material is preserved. From the DOS shown in Fig. 5 it will become clear that the disorder in each graphite layer has indeed led to a transition from the well-known graphite features of the DOS to a metallic DOS.

Fig. 6 presents the advanced stages of the melting process that has started in Fig. 4. We can observe now

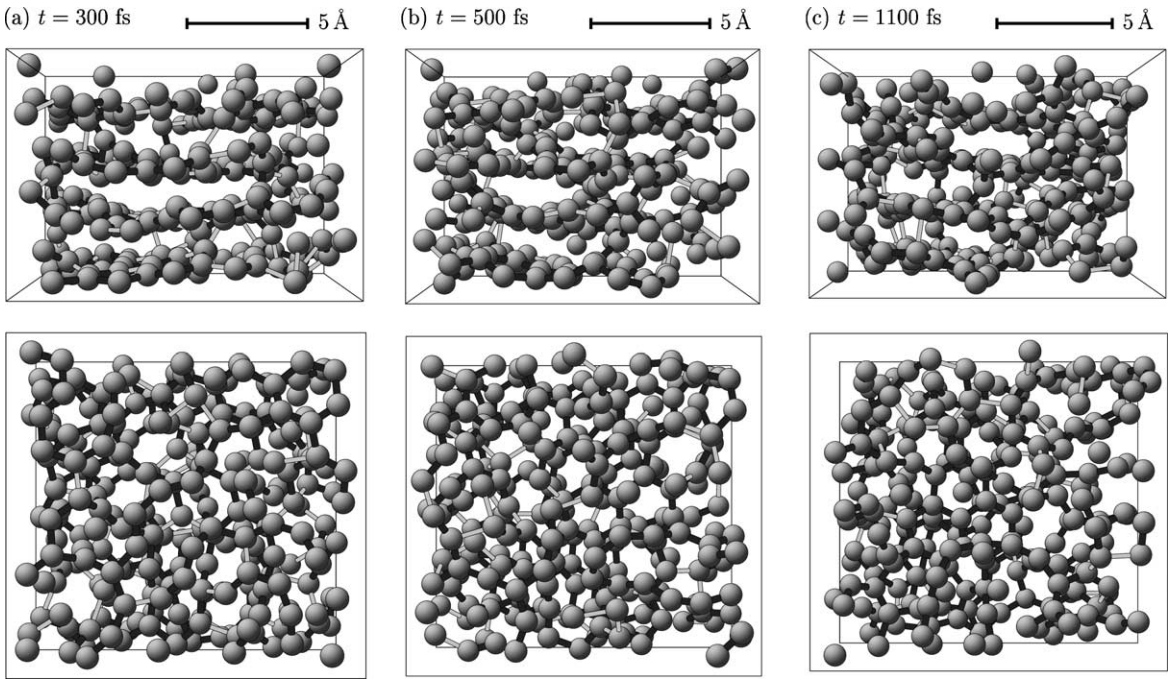

Fig. 6. Advanced stage of the melting of graphite under a pressure of $p = 10$ GPa at an absorbed energy of $E_0 = 3.8$ eV per atom. The pulse duration was $\tau = 20$ fs. At each time the MD unit cell is shown from above and from the side. Bonds up to a length of $l = 1.6$ Å are drawn in dark grey, weaker bonds of $1.6\,\text{Å} < l < 2.0$ Å in light grey. In the advanced stage of melting, atoms invade the space between the graphite planes and the layer structure is lost.

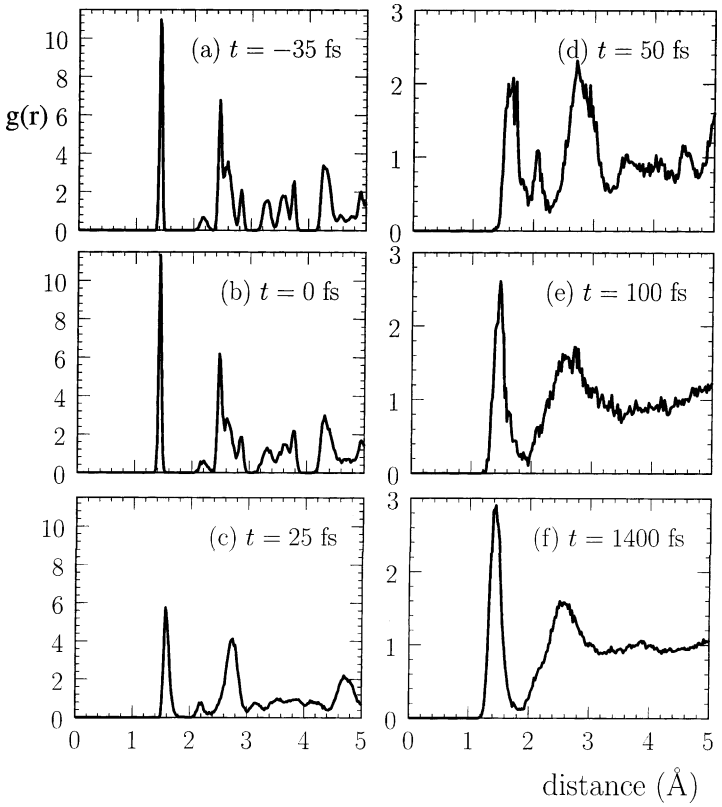

Fig. 7. Pair correlation function $g(r)$ during the melting of graphite under a pressure of $p = 10$ GPa at an absorbed energy of $E_0 = 3.8$ eV per atom. The pulse duration was $\tau = 20$ fs. The time of (a) is negative because we measure time with respect to the laser-pulse maximum. The pair correlation functions correspond to the same trajectory as Figs. 4 and 6. Note, the ordinate scale of the left figures is different from those on the right. At $t = 0$ fs, $g(r)$ is not significantly modified with respect to $g(r)$ before the pulse (see (a)). Already 25 fs after the pulse maximum, the structures of $g(r)$ have significantly broadened. Within 100 fs after the pulse maximum (see (e)), the pair correlation function of liquid carbon is formed.

the gradual loss of the layer structure of the material. While layers are still recognizable at $t = 300$ fs (see Fig. 6a), we observe ever stronger interactions between the graphite planes at $t = 500$ and 1100 fs (see Fig. 6b and c).

In Fig. 7 we show the pair correlation functions $g(r)$ during the melting of carbon under pressure. They are calculated according to

$$g(r) = \frac{\langle \Delta N(r) \rangle}{n_a \, 4\pi \, r^2 \Delta r}, \tag{7}$$

where $\Delta N(r)$ is the number of atoms situated at a distance between r and $r + \Delta r$ around a given particle, and $n_a = N/\Omega$ is the atomic density of the material. The pair correlation functions of Fig. 7 correspond to the same trajectory as Figs. 4 and 6. The $g(r)$ at the pulse maximum (see Fig. 7b) does not yet differ much from $g(r)$ before the pulse (Fig. 7a). But then a rapid broadening of the structures of $g(r)$ occurs (Fig. 7c and d) and at $t = 100$ fs the pair correlation function of liquid carbon has already been formed. This figure confirms the ultrafast, non-thermal character of the melting process in the presence of a dense electron-hole plasma (for which the fraction of excited electrons is $\xi = 12\%$ in this case).

4. Summary

Our molecular dynamics simulations show two distinct processes in the non-equilibrium melting of graphite. In the first stage of approximately 200 fs

duration, the honey comb structure of the graphite layers is destroyed which already creates a metallic-like DOS. The second stage brings the loss of the layered structure of the material on a time scale of approximately 1 ps. This observation sheds light on the difficulties in finding a non-thermal transition from graphite to diamond. The layer structure of graphite is so stable that a laser-induced electron-hole plasma does not lead to an instant "cold" destruction of the layer structure and thus to the formation of a three-dimensional structure. Instead, only after the destruction of order in the graphite layers a melting and dissolution of the layer structure of graphite sets in. The calculations presented in this paper might trigger new time-resolved experimental studies. Time-dependent diffraction using ultrashort X-ray pulses [15] might be an appropriate method to characterize the non-equilibrium ultrafast melting of graphite.

It would be interesting to compare non-equilibrium melting processes at different pressures, pulse durations and laser energies.

Acknowledgements

This work has been supported by the Deutsche Forschungsgemeinschaft through SFB 450. Our simulations were done on the CRAY T3E at Konrad-Zuse-Zentrum für Informationstechnik, Berlin.

References

[1] C.V. Shank, R. Yen, C. Hirlimann, Phys. Rev. Lett. 51 (1983) 900.
[2] D.H. Reitze, H. Ahn, M.C. Downer, Phys. Rev. B 45 (1992) 2677.
[3] P. Stampfli, K.H. Bennemann, Phys. Rev. B 42 (1990) 7163; P. Stampfli, K.H. Bennemann, Phys. Rev. B 49 (1994) 7299.
[4] D.H. Reize, H. Ahn, M.C. Downer, Phys. Rev. B 45 (1992) 2677;
T. Dallas, M. Holtz, H. Ahn, M.C. Downer, Phys. Rev. B 49 (1994) 796.
[5] H.O. Jeschke, M.E. Garcia, K.H. Bennemann, Phys. Rev. B 60 (1999) R3701.
[6] H.O. Jeschke, M.E. Garcia, K.H. Bennemann, Appl. Phys. A 69 (1999) 49.
[7] H.O. Jeschke, M.E. Garcia, K.H. Bennemann, Phys. Rev. Lett. 87 (2001) 015003.
[8] P.L. Silvestrelli, A. Alavi, M. Parrinello, D. Frenkel, Phys. Rev. Lett. 77 (1996) 3149.
[9] K. Sokolowski-Tinten, J. Solis, J. Bialkowski, J. Siegel, C.N. Afonso, D. von der Linde, Phys. Rev. Lett. 81 (1998) 3679.
[10] S. Preuss, M. Stuke, Appl. Phys. Lett. 67 (1995) 338.
[11] K. Sokolowski-Tinten, J. Bialkowski, D. von der Linde, Phys. Rev. B 51 (1995) 14186.
[12] K. Sokolowski-Tinten, J. Bialkowski, A. Cavalleri, D. von der Linde, A. Oparin, J. Meyer-ter-Vehn, S.I. Anisimov, Phys. Rev. Lett. 81 (1998) 224.
[13] K. Sokolowski-Tinten, S. Kudryashov, V. Temnov, J. Bialkowski, D. von der Linde, A. Cavalleri, H.O. Jeschke, M.E. Garcia, K.H. Bennemann, Ultrafast phenomena XI, in: T. Elsaesser et al. (Eds.), Springer Series in Chemical Physics, vol. 66, 2000, p. 425.
[14] J.S. Horwitz, H.-U. Krebs, K. Murakami, M. Stuke (Eds.), Laser ablation, in: Proceedings of the Fifth International Conference, Göttingen, 1999, Appl. Phys. A 69 (7) (1999) S1–S952.
[15] A.M. Lindenberg, I. Kang, S.L. Johnson, T. Missalla, P.A. Heimann, Z. Chang, J. Larsson, P.H. Bucksbaum, H.C. Kapteyn, H.A. Padmore, R.W. Lee, J.S. Wark, R.W. Falcone, Phys. Rev. Lett. 84 (2000) 111.
[16] M. Lenzner, J. Krüger, S. Sartania, Z. Cheng, Ch. Spielmann, G. Mourou, W. Kautek, F. Krausz, Phys. Rev. Lett. 80 (1998) 4076.
[17] H.O. Jeschke, M.E. Garcia, K.H. Bennemann, J. Appl. Phys. 91 (2002) 18.
[18] P.L. Silvestrelli, M. Parrinello, J. Appl. Phys. 83 (1998) 2478.
[19] M. Parrinello, A. Rahman, Phys. Rev. Lett. 45 (1980) 1196.
[20] L. Verlet, Phys. Rev. 159 (1967) 98.
[21] J.N. Glosli, F.H. Ree, Phys. Rev. Lett. 82 (1999) 4659.
[22] D.W. Brenner, Phys. Rev. B 42 (1990) 9458.